Chinese Chemical Letters 33 (2022) 1529–1532

Contents lists available at ScienceDirect

Chinese Chemical Letters

journal homepage: www.elsevier.com/locate/cclet

Host-guest interaction tailored cucurbit[6]uril-based supramolecular organic frameworks (SOFs) for drug delivery

Chun Liu[a], Yu Xia[a], Zhu Tao[a], Xin-Long Ni[a,b,*]

[a] Key Laboratory of Macrocyclic and Supramolecular Chemistry of Guizhou Province, Guizhou University, Guiyang 550025, China
[b] College of Chemistry and Chemical Engineering, Key Laboratory of the Assembly and Application of Organic Functional Molecules of Hunan Province, Hunan Normal University, Changsha 410081, China

ARTICLE INFO

Article history:
Received 8 July 2021
Revised 24 August 2021
Accepted 24 August 2021
Available online 28 August 2021

Keywords:
Cucurbituril
SOFs
Porous materials
Host-guest interaction
Drug delievery

ABSTRACT

An approach for the construction of crystalline porous supramolecular organic frameworks (SOFs) *via* outer-surface interactions of cucurbit[6]uril (Q[6]) with high yield is presented. This approach enables the noncovalent integration of guest molecules into ordered topologies and creates new host–guest-complex-based SOFs; *i.e.*, the topology can be predesigned and constructed by using $[ZnCl_4]^{2-}$ anions to induce the formation of solid Q[6]-SOFs, and the pore wall surface can be easily modified by the Q[6]-encapsulated guest molecules. In addition, one of prepared solid Q[6]-SOFs showed a high drug-loading capacity and smart potential release control for drug-delivery applications

Recent studies have revealed that cucurbit[*n*]urils (Q[*n*]s or CB[*n*]s) [1-7] as macrocyclic organic building blocks exhibit excellent advantages in the construction of various supramolecular organic frameworks (SOFs) [8-13]. For example, Li *et al.* demonstrated the direct preparation of single-layer periodic honeycomb-shaped two-dimensional (2D) SOFs and periodic adamantine-shaped three-dimensional (3D) SOFs [14] with catalysis effect in water through the host-stabilized charge-transfer interactions of various pyridinium derivatives with Q[8]s. Cao *et al.* reported the fabrication of cellular-imaging fluorescent 3D SOFs from 2D networks *via* Q[8]-based host–guest interactions in an acidic aqueous solution [15]. In this approach, the Q[8] host molecules act as molecular handcuffs to simultaneously include two guest molecules in each host cavity, thus, forming the SOFs in solution

We reported that Q[*n*]s can be used as rigid cage blocks to produce a variety of Q[*n*]-based solid SOFs (QSOFs) [16-18], including self-induced, anion-induced, and aromatic-compound-induced QSOFs with unique adsorption properties, through outer-surface interactions [19-21]. Generally, the driving forces for the assembly of QSOFs are mainly weak noncovalent interactions such as C-H$\cdots\pi$ and ion−dipole interactions from the positive electrostatic potential of the outer surface of Q[*n*]s; importantly, these QSOFs can be quickly crystallized from the solution. Stoddart [22] and our group [23,24] independently used this approach to develop a facile strategy for high-efficiency gold recovery in acidic aqueous solutions. However, there are few reports on the host–guest-complex-derived solid QSOFs, which are formed by exploiting the outer-surface interactions of Q[*n*]s. In 2017, we successfully obtained the first example of solid 3D polycatenanes formed *via* Q[6] host–guest interactions [25], which was stabilized by the outer-surface interactions between Q[6] and $[CdCl_4]^{2-}$ anions and could be rapidly precipitated from the solution mixture with a high yield. From a structure viewpoint, the simple and low cost of the outer-surface interactions triggered solid SOFs from the host-guest interaction of Q[*n*] cavity with various functional guest molecules could be one of ideal complementary approach for construction of modification of MOFs [26,27] and COFs [28], because the modification can enhance many of new properties and functions of the parent species.

In this study, as a proof of concept, a series of Q[6]-based solid SOFs with empty cavities (Q[6]-SOF-**1** and Q[6]-SOF-**1b**) and guest encapsulation in the Q[6] molecules (Q[6]-SOF-**2** and Q[6]-SOF-**3**) were successfully prepared with a high yield in the presence of $[ZnCl_4]^{2-}$ anions as the structure inducer. After evaluation in a wide range of experimental conditions, the host–guest interaction of Q[6] with 2-(cyclohexylamino)ethanol (*N*-ECyA)-derived Q[6]-SOF-**2** was explored for drug-loading applications (*e.g.*, for loading ibuprofen (IBU)); Q[6]-SOF-**2** exhibited smart temperature- and pH-sensitive IBU release, due to the reversible weak noncovalent interactions of QSOF-**2** assemblies. This result shows that the as-

* Corresponding author at: Key Laboratory of Macrocyclic and Supramolecular Chemistry of Guizhou Province, Guizhou University, Guiyang 550025, China.
E-mail address: longni333@163.com (X.-L. Ni).

https://doi.org/10.1016/j.cclet.2021.08.108
1001-8417/

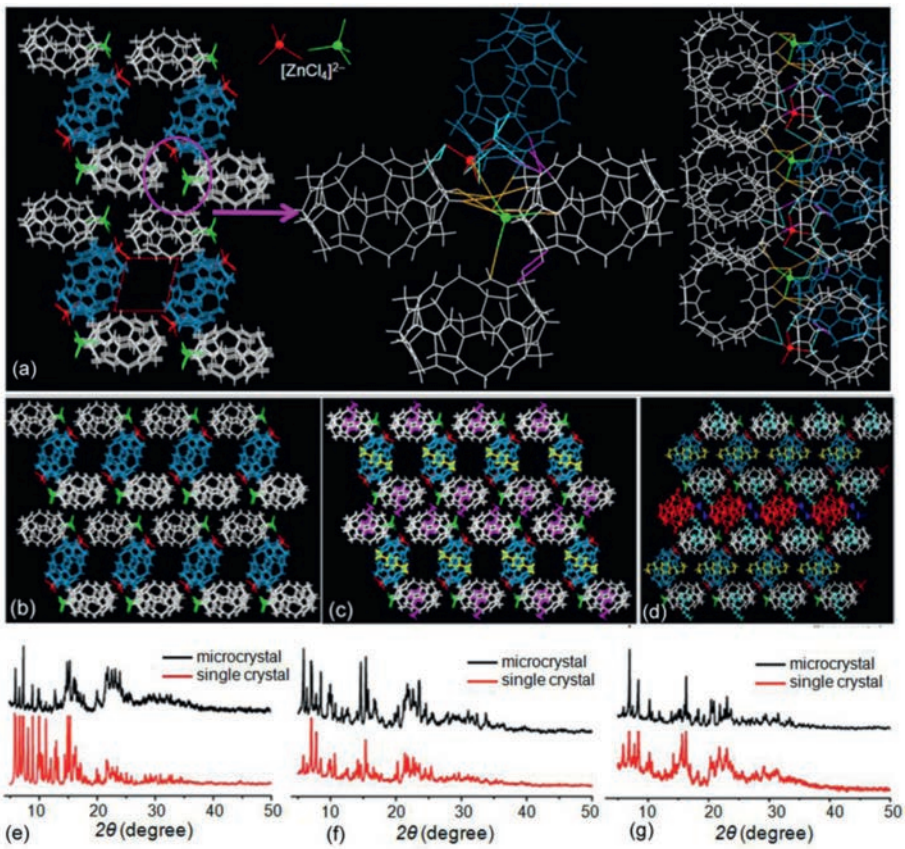

Fig. 1. Crystal structures of Q[6]-SOFs: (a) $[ZnCl_4]^{2-}$-induced outer-surface interactions of Q[6] in Q[6]-SOF-**1**. Overall view of tetragonal channels along the *a* axis in (b) Q[6]-SOF-**1**, (c) Q[6]-SOF-**2**, and (d) Q[6]-SOF-**3**; XRD pattern of microcrystal and single crystal of (e) Q[6]-SOF-**1**; (f) Q[6]-SOF-**2**; (g) Q[6]-SOF-**3**.

sembly of host–guest complexes triggered by the outer-surface interactions of Q[*n*]s and the dynamic non-covalent interactions provide new construction and application models of SOFs. Furthermore, the results of this study reveal that the electrostatic potential of the Q[6] host can be tailored *via* guest inclusion, which provides a new avenue for developments in macrocycle-based porous materials.

Typically, ion–dipole interactions between the positive-electropotential outer surface of Q[*n*] host molecule and $[CdCl_4]^{2-}$ anion is the mainly driving force for the construction of solid Q[*n*]-SOFs from a hydrochloric acid solution. However, the toxicity of Cd^{2+} ions greatly limits their applications. The $[ZnCl_4]^{2-}$ anion is a good alternative to the $[CdCl_4]^{2-}$ anion, however, when $[ZnCl_4]^{2-}$ ions are used, the rapid production of a large amount of crystallized QSOFs from solution (as in the case of $[CdCl_4]^{2-}$ anions) is difficult [24]. After many attempts, we found that a high concentration of HCl (> 4.0 mol/L) is beneficial to the crystallization of $[ZnCl_4]^{2-}$-induced Q[6]-SOFs (Supporting information). In this study, Q[6] was dissolved in a 6.0 mol/L HCl solution in the presence and absence of 1.0 equiv. of guest *N*-(3-aminopropyl)cyclohexylamine (*N*-ACyA) and *N*-(2-hydroxyethyl)cyclohexylamine (*N*-ECyA), and then, 6.0 equiv. of $ZnCl_2$ (in a 6.0 mol/L HCl solution) was added to the solution. A large number of microcrystals were precipitated within a short time (2 h) with a yield of 50% to 75%. The empty Q[6]-based, Q[6]-*N*-ECyA complex based, and Q[6]-*N*-ACyA complex based microcrystals were denoted Q[6]-SOF-**1**, Q[6]-SOF-**2**, and Q[6]-SOF-**3**, respectively. X-ray quality crystals were obtained from the filtrate solution within 2–3 days. The X-ray diffraction analysis revealed that all the Q[6]-SOFs have the same triclinic crystal system with the same *P*-1 space group and similar cell parameters with slightly different unit cell parameters (Table S1 in Supporting information). In addition, the powder X-ray diffraction (PXRD) pattern of each Q[6]-SOF matches the corresponding single-crystal-based simulated pattern, indicating the formation of pure-phase crystalline products (Figs. 1e-g).

Figs. 1a-d show an overview of the network of Q[6]-SOFs in the solid state. As can be seen from Fig. 1a, the supramolecular assembly of Q[6]-SOF-**1** is mainly driven by the ion–dipole interactions (C–H···Cl, green and orange color) between the positive-electropotential outer surface of Q[6] molecules and $[ZnCl_4]^{2-}$ anions, and by an additional ion–dipole interaction (C–H···O, purple color) between the portal carbonyl oxygen of the Q[6] molecule and the positive-electropotential outer surface of adjacent Q[6] molecules. Thus, Q[6]-SOF-**1** was formed, and the overall stacking of this assembly occurred *via* a combination of the aforementioned intermolecular interactions. In particular, the empty Q[6] molecules seemed to be held by $[ZnCl_4]^{2-}$ anions and are perfectly arranged in a 1D tetragonal channel (constructed by $[ZnCl_4]^{2-}$, in red color) in a layered manner (linked by $[ZnCl_4]^{2-}$, in green color) along the *a* axis (Fig. 1b and Figs. S1 and S2 in Supporting informaiton), where the carbonyl portals of the Q[6] molecules face the channel wall. Closer inspection reveals the empty Q[6]-based tetragonal 1D channels with a cross-sectional area of about 90 $Å^2$ (9.0 Å × 10.0 Å). Similar supramolecular assemblies like Q[6]-SOF-**1** can be observed in the X-ray structures of Q[6]-SOF-**2** (Fig. 1c and Fig. S3 in Supporting information) and Q[6]-SOF-**3** (Fig. 1d and Fig. S4 in Supporting information), respectively. However, one set of the host–guest complex of Q[6]@*N*-ACyA (red color) separates each row of tetragonal channels in Q[6]-SOF-**3** in a regular fence-like manner (Fig. 1d). In addition, the guest molecules in one set of the host–guest assembly (yellow color) of Q[6]-SOF-**2** and Q[6]-

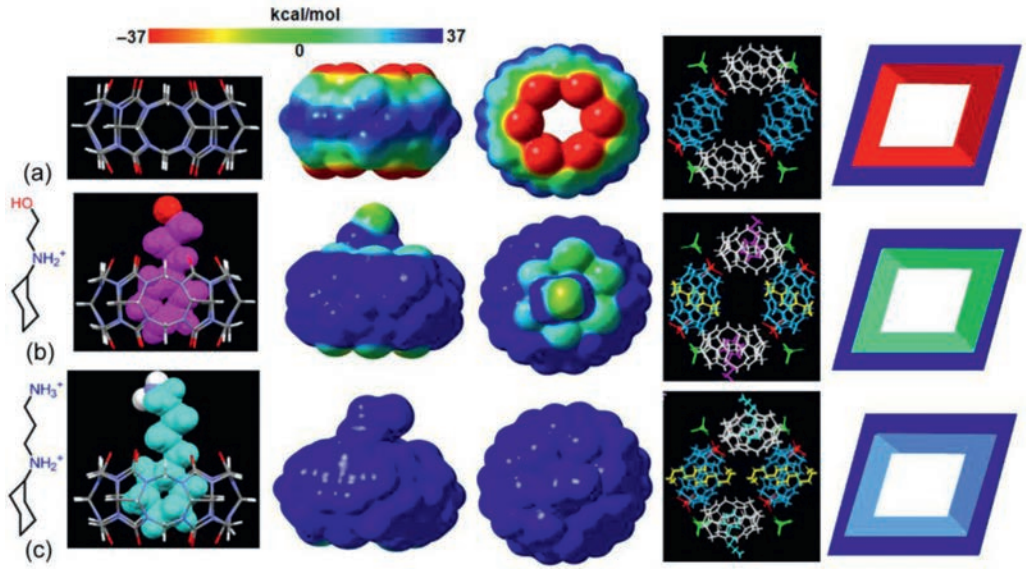

Fig. 2. Electrostatic potential maps (ESPs): (a) empty Q[6], (b) Q[6]@*N*-ECyA complex, (c) Q[6]@*N*-ACyA complex, and cartoon presentation of the resulting tetragonal channels in SOFs. ESPs was performed at the B3LYP/6–311 G (d, p) level of theory with Gaussian 16.

SOF-**3** show disorder owing to the 1:1 complex caused randomness of the guest towards the portals of Q[6].

The above results indicate that the $[ZnCl_4]^{2-}$anions as the structure inducer play a key role in controlling the assembly structure and promoting the crystallization of all the Q[6]-SOFs. In other words, in the HCl solution, the numerous negatively charged $[ZnCl_4]^{2-}$ act as anchors to hold the Q[6] molecules, including the Q[6]-based host–guest complex, through electrostatic interactions with the electrostatically positive outer surface of the Q[6] host. Unexpectedly, the electrostatic potential surface maps (ESPs) suggested that a similar electrostatically positive appeared on both the outer surface of empty Q[6] and the Q[6]-based host–guest complex, but the intensity of the positive potential of Q[6] obviously increased upon complex formation with the protonation guest molecules (Fig. 2). In particular, an electrostatically positive seems to cover the full host–guest system of the Q[6]@*N*-ACyA complex (Fig. 2c). This result suggested that the electrostatic potential of the whole Q[*n*] molecules can be tunable by the encapsulated guests, which will help in the development of crystalline host–guest complexes from solution. As a result, a significantly negative charge was seen on the carbonyl portals of empty Q[6]s, a neutral charge was observed in the Q[6]-*N*-ECyA complex, and a positive charge emerged in the whole Q[6]-*N*-ACyA complex. In other words, the remarkable difference in the electrostatic force on the portals of Q[6] and the Q[6] host–guest complex makes the tetragonal channels composed of the Q[6]-SOFs exhibit different properties: the negative charge of the channels of Q[6]-SOF-**1** (derived from the negatively charged carbonyl atoms), neutral charge of the channels of Q[6]-SOF-**2** (derived from the terminal neutral –OH moiety of *N*-ECyA), and positive charge of the channels of Q[6]-SOF-**3** (derived from the terminal positive charged $-NH_3^+$moiety of *N*-ACyA).

We exploited the tetragonal channels in the empty Q[6]-SOF-**1** and in Q[6]-SOF-**2** and Q[6]-SOF-**3** for controlling drug delivery *in vitro*. IBU is well known as a nonsteroidal anti-inflammatory drug and is widely used to treat inflammation, pain, and rheumatism [29]. In particular, in recent years, it is commonly used to treat fever caused by the common cold or influenza in children. However, the drug has a short biological half-life (2 h) [30], which makes it a candidate for sustained or controlled drug delivery. In this study, IBU was selected as a model drug because the pore size and the deep cavities of the Q[6]-SOFs were expected to enable the "comfortable" entrapment of IBU (molecular size: 5 Å × 10 Å) [31]. To load the drug, the activated Q[6]-SOFs were immersed in an IBU–hexane solution at room temperature overnight, filtered, and washed with hexane (Supporting information). UV–vis absorption spectra indicated that only Q[6]-SOF-**2** can load IBU (Fig. S5b in Supporting information). The resultant PXRD peaks coincide with those of the starting material, confirming the structural integrity after loading (Fig. S6 in Supporting information). Therefore, the successfully loading of IBU in Q[6]-SOF-**2** can be attributed to the neutral channels of Q[6]-SOF-**2**, which may facilitate the adsorption of neutral IBU molecules like CDs whose portal and cavity are almost neutral [32,33]. In particular, the ethanol moiety of *N*-ECyA that remains exposed outside the portal of Q[6] perhaps further stabilizes the IBU molecule through hydrogen bonds and van der Waals forces. In Q[6]-SOF-**3**, the positive charge channel may benefit to the capture of IBU, but the more protruded tail of the guest partially fills the channel (Fig. 2c) sterically hindering the uptake.

The amount of IBU in IBU-loaded Q[6]-SOFs-**2** was evaluated at concentrations of 26.9 wt%, based on the UV–vis absorption spectra (Fig. S5 in Supporting information). The drug-release profiles were also obtained by performing the UV–vis absorption experiment and using a calibration curve for IBU. In order to assess the suitability of Q[6]-SOFs-**2** for practical applications, the solid IBU-loaded Q[6]-SOFs-**2** sample was first soaked in simulated body fluid (SBF) solution (pH 7.4) at 37 °C, and the IBU absorbance was monitored at different time intervals. As shown in Fig. 3, the UV–vis spectra of IBU-loaded Q[6]-SOFs-**2** showed a typical IBU absorption peak around 257 nm and 265 nm, and the peak intensity gradually increased with time, suggesting that the amount of IBU released from the solid Q[6]-SOFs-**2** into water increases with time. Overall, the corresponding intensity curve of IBU indicated that the concentration of IBU slowly increased for 600 min, indicating that the drug-loaded particles released the drug at a slow rate. After 600 min, no discernible change in concentration was observed. In addition, taking into account the elevated temperature of patients with fever and the weakly acidic nature of body fluids, the drug-release experiment was performed in neutral and acidic SBF solutions at 40 °C. Most of the IBU was released within about

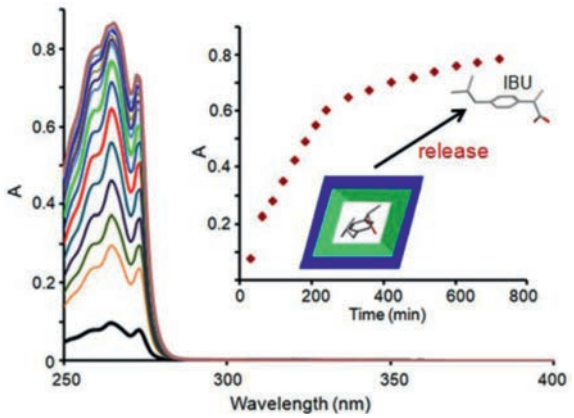

Fig. 3. UV–vis absorption spectra of IBU-loaded Q[6]-SOFs-**2** in simulated body fluid solution (pH 7.4) at 37 °C in different times. Inset: IBU release profiles with times.

300 min in neutral system (Fig. S7 in Supporting information), and was fast released within 180 min in the acidic environment (Fig. S8 in Supporting information), which correspond to higher drug-release rates than that at 37 °C; thus, the drug delivery in patients with fever will be faster.

In summary, we have prepared novel host–guest-complex-based solid Q[6]-SOFs by exploiting the outer-surface interactions of Q[6]s; that is, the topology structure and pore sizes can be predesigned and constructed by using the $[ZnCl_4]^{2-}$-induced SOFs, and the pore wall surface can be easily regulated and functionalized using the macrocycle-encapsulated guest. In particular, the guest inclusion is shown to significantly modify the electrostatic potential of the Q[6] molecules, which thereby provides a new approach for advancements in macrocycle-based host–guest chemistry, *e.g.*, in promoting the crystallization of host–guest complex. Furthermore, the smart pH- and temperature-sensitive drug delivery of Q[6]-SOF-**2** in water indicated that the formation of reversible weak noncovalent bonds of Q[*n*]-SOFs, triggered by the outer-surface interactions, has potential pharmaceutical applications.

Declaration of competing interest

The authors declare no competing financial interest.

Acknowledgments

This work was supported by the National Natural Science Foundation of China (No. 21871063), the Science and Technology Foundation of Hunan Province (No. 2020JJ2021), and the high performance computing platform of Guizhou University.

Supplementary materials

Supplementary material associated with this article can be found, in the online version, at doi:10.1016/j.cclet.2021.08.108.

References

[1] J. Kim, I.S. Jung, S.Y. Kim, et al., J. Am. Chem. Soc. 122 (2000) 540–541.
[2] A. Day, A.P. Arnold, R.J. Blanch, B. Snushall, J. Org. Chem. 66 (2001) 8094–8100.
[3] S.J. Barrow, S. Kasera, M.J. Rowland, J. del Barrio, O.A. Scherman, Chem. Rev. 115 (2015) 12320–12406.
[4] R.N. Dsouza, U. Pischel, W.M. Nau, Chem. Rev. 111 (2011) 7941–7980.
[5] C.L. Deng, S.L. Murkli, L. Isaacs, Chem. Soc. Rev. 49 (2020) 7516–7532.
[6] J. Murray, K. Kim, T. Ogoshi, W. Yao, B.C. Gibb, Chem. Soc. Rev. 46 (2017) 2479–2496.
[7] X.L. Ni, S. Chen, Y. Yang, Z. Tao, J. Am. Chem. Soc. 138 (2016) 6177–6183.
[8] M. Pfeffermann, R. Dong, R. Graf, et al., J. Am. Chem. Soc. 137 (2015) 14525–14532.
[9] C.C. Zhang, X. Liu, Y.P. Liu, Y. Liu, Chem. Mater. 32 (2020) 8724–8732.
[10] H. Bai, Z. Liu, T. Zhang, et al., ACS Nano 14 (2020) 7552–7563.
[11] S.Q. Xu, X. Zhang, C.B. Nie, et al., Chem. Commun. 51 (2015) 16417–16420.
[12] J. Tian, H. Wang, D.W. Zhang, et al., Natl. Sci. Rev. 4 (2017) 426–436.
[13] K.D. Zhang, J. Tian, D. Hanifi, et al., J. Am. Chem. Soc. 135 (2013) 17913–17918.
[14] J. Tian, T.Y. Zhou, S.C. Zhang, et al., Nat. Comm. 5 (2014) 5574.
[15] Y. Li, Y. Dong, X. Miao, et al., Angew. Chem. Int. Ed. 57 (2018) 729–733.
[16] X.L. Ni, X. Xiao, H. Cong, et al., Acc. Chem. Res. 47 (2014) 1386–1395.
[17] Y. Huang, R.H. Gao, M. Liu, et al., Angew. Chem. Int. Ed. 60 (2021) 2–28.
[18] C. Liu, R. Gao, Y. Zhang, et al., Chin. Chem. Lett. 32 (2021) 362–366.
[19] Y.Q. Yao, Y.J. Zhang, C. Huang, et al., Chem. Mater. 29 (2017) 5468–5472.
[20] Y.Q. Yao, Y.J. Zhang, Y.Q. Zhang, et al., ACS Appl. Mater. Interfaces 9 (2017) 40760–40765.
[21] M. Liu, L. Chen, P. Shan, et al., ACS Appl. Mater. Interfaces 13 (2021) 7434–7442.
[22] H. Wu, L.O. Jones, Y. Wang, et al., ACS Appl. Mater. Interfaces 12 (2020) 38768–38777.
[23] L.X. Chen, M. Liu, Y.Q. Zhang, et al., Chem. Commun. 55 (2019) 14271–14274.
[24] R.L. Lin, Y.P. Dong, M. Tang, et al., Inorg. Chem. 59 (2020) 3850–3855.
[25] X. Cui, W. Zhao, K. Chen, et al., Chem. Eur. J. 23 (2017) 2759–2763.
[26] S. Mandal, S. Natarajan, P. Mani, et al., Adv. Funct. Mater. (2020) 2006291.
[27] J. Liao, S. Zhang, Z. Wang, Green Synth. Catal. 1 (2020) 121–133.
[28] Z. Li, T. He, Y. Gong, D. Jiang, Acc. Chem. Res. 53 (2020) 1672–1685.
[29] T. Wyss-Coray, L. Mucke, Nat. Med. 6 (2000) 973–974.
[30] M. Vallet-Regi, A. Rámila, R.P. del Real, J. Pérez-Pariente, Chem. Mater. 13 (2001) 308–311.
[31] F. Highton, The pharmaceutics of Ibuprofen, in: K.D. Rainsford (Ed.), Ibuprofen: A Critical Bibliographic Review, Taylor & Francis London, 1999, p. 53.
[32] D. Shetty, J.K. Khedkar, K.M. Parkad, K. Kim, Chem. Soc. Rev. 44 (2015) 8747–8761.
[33] M. Rao, W. Wu, C. Yang, Green Synth. Catal. 2 (2021) 131–144.